




## Article

# Waste and Solar Energy: An Eco-Friendly Way for Glass Melting

Isabel Padilla <sup>1</sup>, Maximina Romero <sup>1</sup>, José I. Robla <sup>2</sup> and Aurora López-Delgado <sup>3,\*</sup>

<sup>1</sup> MEDES-IETcc Group, Eduardo Torroja Institute for Construction Sciences, IETcc-CSIC. C/Serrano Galvache, 4, 28033 Madrid, Spain; isabel.padilla@ietcc.csic.es (I.P.); mromero@ietcc.csic.es (M.R.)

<sup>2</sup> PROMESS Group, National Centre for Metallurgical Research, CENIM-CSIC. Av. Gregorio del Amo, 8, 28040 Madrid, Spain; jrobla@cenim.csic.es

<sup>3</sup> MEDES-CENIM Group, National Centre for Metallurgical Research, CENIM-CSIC. Av. Gregorio del Amo, 8, 28040 Madrid, Spain

\* Correspondence: alopezdelgado@cenim.csic.es

**Abstract:** In this work, concentrated solar energy (CSE) was applied to an energy-intensive process such as the vitrification of waste with the aim of manufacturing glasses. Different types of waste were used as raw materials: a hazardous waste from the aluminum industry as aluminum source; two residues from the food industry (eggshell and mussel shell) and dolomite ore as calcium source; quartz sand was also employed as glass network former. The use of CSE allowed obtaining glasses in the SiO<sub>2</sub>-Al<sub>2</sub>O<sub>3</sub>-CaO system at exposure time as short as 15 min. The raw materials, their mixtures, and the resulting glasses were characterized by means of X-ray fluorescence, X-ray diffraction, and differential thermal analysis. The feasibility of combining a renewable energy, as solar energy and different waste for the manufacture of glasses, would highly contribute to circular economy and environmental sustainability.

**Keywords:** concentrated solar energy; aluminum industry waste; food industry residue; calcium silicoaluminate glasses



**Citation:** Padilla, I.; Romero, M.; Robla, J.I.; López-Delgado, A. Waste and Solar Energy: An Eco-Friendly Way for Glass Melting. *ChemEngineering* **2021**, *5*, 16. <https://doi.org/10.3390/chemengineering5020016>

Academic Editor: Alirio E. Rodrigues

Received: 4 November 2020

Accepted: 6 April 2021

Published: 8 April 2021

**Publisher's Note:** MDPI stays neutral with regard to jurisdictional claims in published maps and institutional affiliations.



**Copyright:** © 2021 by the authors. Licensee MDPI, Basel, Switzerland. This article is an open access article distributed under the terms and conditions of the Creative Commons Attribution (CC BY) license (<https://creativecommons.org/licenses/by/4.0/>).

## 1. Introduction

In recent decades, great efforts are being conducted to use of renewable and less polluting energy systems in energy-intensive demanding processes, in intent of reducing greenhouse gas emissions into the atmosphere. In this regard, special attention is being focused on the application of concentrated solar energy (CSE) to high temperature production processes [1]. Among others, the glass industry is a highly energy-intensive consumer because of the high temperature required for the glass melting process. Scalet et al. [2] reported that the energy consumption in the glass industry ranges from 3.5 to 40 GJ t<sup>-1</sup>, depending on the production level, furnace design, etc.; the melting of raw materials consumes around 75% of that energy requirement. Fossil fuel combustion is generally used by this industry to reach the high heat demand of the glass melting process, which represents a huge contribution to the global carbon footprint. Nowadays, according to the American National Oceanic and Atmospheric Administration, 414 ppm of global CO<sub>2</sub> was recorded for February 2021 [3]. Upon this alarming situation, changes in the production systems must be highly considered, specially taking into consideration the United Nations Sustainable Development Goals for 2030 (Goals 7- Affordable and Clean Energy, and 13- Climate Action) [4].

The first studies related to the synthesis of glasses from chemical reagents and, by using concentrated solar energy were conducted in the 1980s [5–7] nevertheless, this research line has been barely developed since then. Recently, Romero et al. [8] studied the production of glass frits from chemical reagents by using concentrated solar energy. The results highlighted that glass frits melted by CSE showed similar features when compared to those manufactured in an electric furnace; furthermore, the process allowed reducing

the melting time in about 80%, which results in both less corrosion of the crucible wall and less volatilization of boron during the melting process.

From an environmental point of view, the increase of industrial activities, according to the increase in population and economic growth, presents negative impacts not only due to the alarming increase of the global CO<sub>2</sub> level as above commented, but also because of the management of the vast amount and heterogeneity of the industrial waste generated. Vitrification of waste has been widely used, for decades, to render inert materials [9–11]. It is a well-established technology for the treatment of waste with excellent advantages, such as the treatment of different type of waste, a huge reduction of volume, the immobilization of hazardous elements into the glassy matrix, etc., [12]. Nevertheless, the high energy consumption of the melting process advises against its use for waste inertization, except in the case of radioactive residues [9]. With the objective of combining the use of renewable energy and industrial waste to obtain value-added materials, the purpose of the present work is to study the application of concentrated solar radiation to the manufacture of glasses, from different types of industrial waste as raw materials. A hazardous aluminum waste was used as source of alumina and two residues from the food industry (eggshell and mussel shells) were used as source of calcium oxide. Dolomite ore was also employed as calcium source. Additionally, quartz sand was added as network former to improve the stability of glasses in the SiO<sub>2</sub>-Al<sub>2</sub>O<sub>3</sub>-CaO system [9,13–15]. This ternary system was selected because of the wide compositional range for glass formation, and also due to the wide application fields of glasses in this system (glassware, windows glass, ceramic glazes, etc.) [16,17].

The aluminum waste consists of a powdered solid trapped in filter sleeves during the slag milling process in the aluminum tertiary industry. This waste is currently disposed in safe storage facilities because of its hazardousness and scarce commercial value [18]. Its classification as hazardous waste is due to the high aluminum content as metallic aluminum or aluminum nitride. These compounds can react in a very low humidity atmosphere to release toxic or dangerous gases such as hydrogen and ammonia. Previous works have demonstrated the feasibility of non-metallic waste from aluminum secondary industry to form glasses in a mixture with SiO<sub>2</sub> and CaCO<sub>3</sub> (chemical reagents), to inertize this hazardous waste into a glassy matrix [9]. Furthermore, it was demonstrated that glasses obtained from this aluminum-rich waste exhibited similar characteristic to those obtained with chemical reagents [16]. A recent work has also reported the development of sintered glass-ceramic tiles by the sinter-crystallization of mixtures composed of aluminum slag and reclaimed packaging glass [19].

However, remarkable differences can be found between the previous papers and this work. The studies early reported deal either with the vitrification of waste by conventional processes (electric energy) or with the manufacturing of glasses by CSE but from pure raw materials. However, to our knowledge, the combination of CSE and waste as raw materials has not previously been investigated. Therefore, the aim of this paper is the synthesis of glasses in the SiO<sub>2</sub>-Al<sub>2</sub>O<sub>3</sub>-CaO system from different wastes as raw materials and using concentrated solar energy to provide the energy required for the melting process.

## 2. Materials and Methods

### 2.1. Materials

The raw materials used to prepare glasses were the following: an aluminum waste from the tertiary aluminum industry (AW) as the source of aluminum; eggshells (ES), mussel shells (MS), and natural dolomite (DO) as calcium source; and quartz sand (QS) as silica source. In order to prepare the samples for the treatment with CSE, aluminum waste (25 wt.%), eggshell, mussels shell or dolomite (50 wt.%), and quartz sand (25 wt.%) were mixed and homogenized in a ball mill for 15 min. The raw materials were previously milled (<300 μm). Then, the mixtures (3 g) were compacted in a press at 3 ton for 3 min. Disks of 13 mm diameter and 2 mm height were obtained for the subsequent treatment in the concentrated solar radiation facility. The initial mixtures are named as M<sub>i</sub>-ES, M<sub>i</sub>-MS, and M<sub>i</sub>-DO, to indicate the source of calcium oxide (eggshell, mussel shell, or dolomite).

## 2.2. Characterization Techniques

The chemical composition of the raw materials and glasses was determined by X-ray fluorescence (XRF) using a Bruker S8 Tiger spectrometer. The analysis was performed on pressed pellets of powder samples (<63  $\mu\text{m}$ ). The evaluation of the mineralogy of raw materials and the amorphous or crystalline nature of the melt resulting products was performed by X-ray diffraction (XRD) using Bruker D8 Advance equipment with Ni-filtered Cu K $\alpha$  radiation operating at 30 mA and 40 kV. Data were recorded in the 5–60° 2 $\theta$  range (step size 0.019732° and 0.5 s counting time for each step). The percentage of crystallinity of the glasses obtained by CSE was determined semi-quantitatively by the DIFFRAC EVA v4.2 software. The thermal behavior of the initial mixtures and the thermal stability of the glasses were analyzed by differential thermal analysis (DTA) up to 1200 °C, at a heating rate of 50 °C min<sup>-1</sup> under air flow in a Setaram Labsys Thermal Analyzer. The samples (40 mg) were placed in platinum crucibles and calcined Al<sub>2</sub>O<sub>3</sub> was used as the reference material. The DTA curves were normalized to the sample weight.

## 2.3. Method

Melting experiments were performed in the Medium Size Solar Furnace (MSSF) of the CNRS-PROMESS Solar facilities (Font Romeu-Odeillo, France) [20]. The solar furnace of 0.9 kW consisted of a vertical axis parabolic reflector of 1.5 m diameter, which produces a focal spot, ca. 15 mm in diameter, with a very high power density (1000 W m<sup>-2</sup>). To control the incident solar radiation, a shutter is positioned between the parabolic concentrator (placed on the 6th floor level) and the heliostat (placed on the 1st floor level). This vertical configuration is the only one that allows the melting of glasses without spilling the liquid phase [8]. Figure 1 shows the crucible receiving the solar radiation concentrated by the parabolic reflector, the heliostat, and a detail of the shutter.

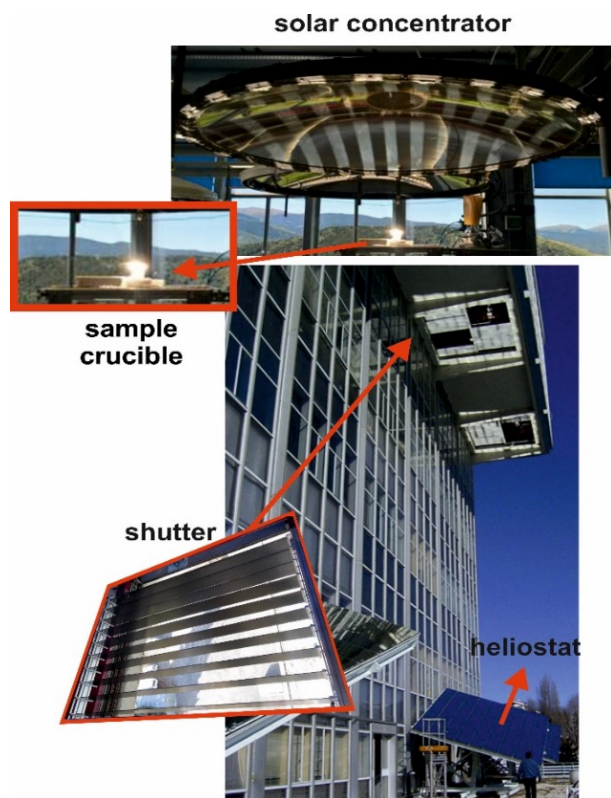
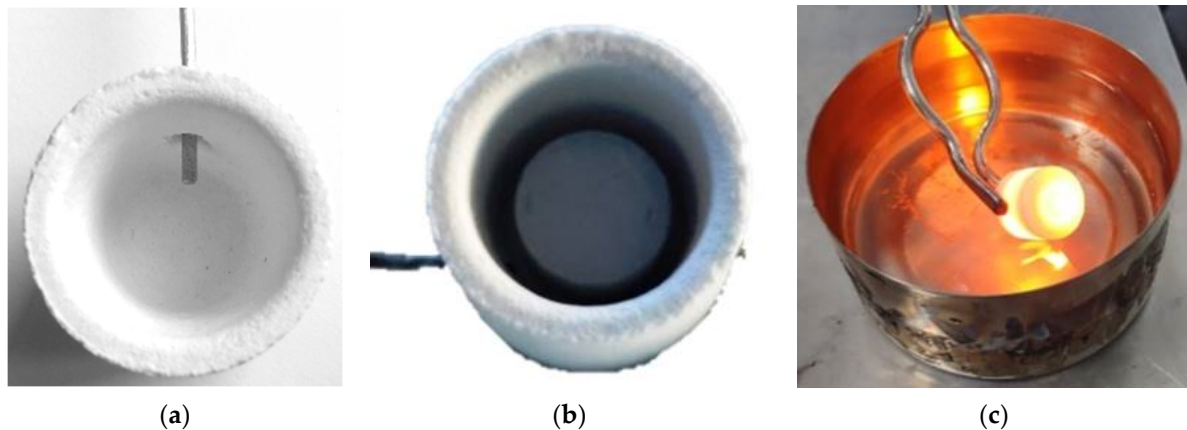


Figure 1. Solar energy facility (CNRS, Odeillo, France).

The direct solar irradiation during the experiments was quasi-steady, and values between 810 and 870 W m<sup>-2</sup> were registered. The samples were placed into cylindrical

mullite-feldspar-alumina crucibles (22 mm diameter and 25 mm height). A small hole was drilled in the wall of the crucible at mid-height, so that a type K thermocouple could be inserted to record the temperature (Figure 2).



**Figure 2.** View of crucible with, (a) thermocouple insertion, (b) initial sample disk, and (c) quenching into cold water after treatment.

The shutter was partially opened (20–30%) at the beginning of the experiments to avoid an abrupt increase of the temperature on the sample; immediately after, the shutter was progressively opened until it was fully open. The samples were subjected to a fast-melting process. The periods of exposure to solar radiation from room temperature to pouring, were 5, 10, and 15 min. Table 1 collects the experimental conditions related to the shutter opening percentage and the time of exposure to concentrated solar radiation for the melting of the different samples. Once the period of exposure was finished, the shutter was suddenly closed and the melts were quenched into cold water (Figure 2c). The samples obtained by CSE are, hereinafter named as  $M_x$ -ES,  $M_x$ -MS,  $M_x$ -DO, where  $x$  is the time of exposure to solar radiation (5, 10, 15 min).

**Table 1.** Experimental conditions for the exposure of samples to concentrated solar radiation.

| Shutter Opening (%)      | Power (W) | Exposure Time (min)                 |  |  |
|--------------------------|-----------|-------------------------------------|--|--|
|                          |           | $M_5$ -ES<br>$M_5$ -MS<br>$M_5$ -DO | $M_{10}$ -ES<br>$M_{10}$ -MS<br>$M_{10}$ -DO | $M_{15}$ -ES<br>$M_{15}$ -MS<br>$M_{15}$ -DO |
| 20                       | 90        | -                                   | 1  | 1  |
| 30                       | 150       | 1                                   | 1  | 1  |
| 50                       | 350       | 1                                   | 3  | 5  |
| 70                       | 600       | 1                                   | 2  | 6  |
| 100                      | 970       | 2                                   | 3  | 2  |
| $t_{\text{total}}$ (min) |           | 5                                   | 10   | 15   |

The temperature–time registers during the experiments of melting by CSE are shown in Figure 3 (as an example, the graphs of samples  $M_x$ -ES are depicted). It should be noted that the temperature recorded by the thermocouple corresponds to that of its position at mid-height of the crucible, and can only be recorded up to about 1300 °C due to the limitations of the thermocouple itself. Nevertheless, it is estimated that temperatures higher than 1500 °C were reached [5,7], as it will be discussed below. According to this figure, the heating rate (from room temperature up to 800 °C) was quite similar for samples treated for 10 and 15 min ( $\sim 1.6$  °C  $s^{-1}$ ). For the sample treated for 5 min, the heating rate was much faster ( $\sim 3.7$  °C  $s^{-1}$ ).



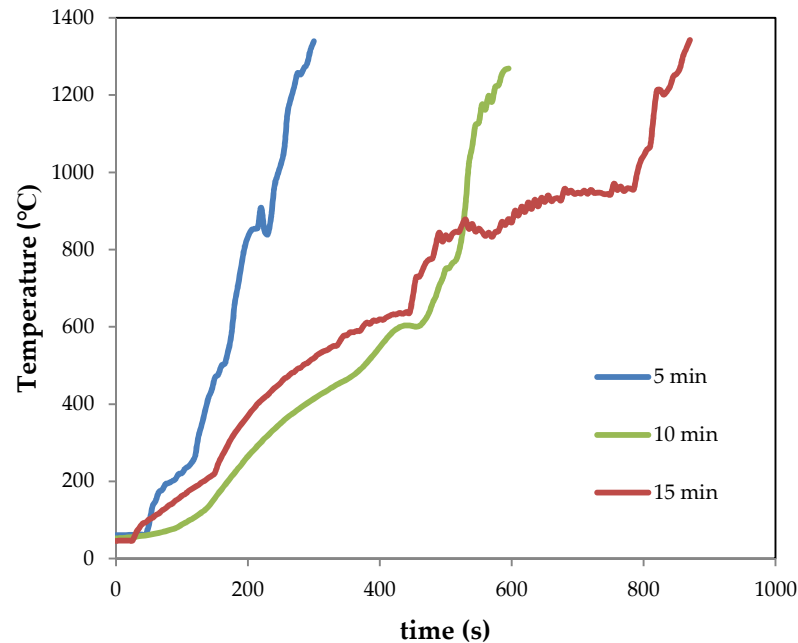


**Figure 3.** Temperature–time registers for samples M<sub>5</sub>-ES, M<sub>10</sub>-ES, M<sub>15</sub>-ES.

### 3. Results and Discussion

#### 3.1. Characterization of Raw Materials

The chemical composition of the raw materials used to prepare the mixtures to be melted by CSE, is collected in Table 2.

**Table 2.** Main chemical composition of aluminum waste (AW), eggshells (ES), mussel shells (MS), dolomite (DO), and quartz sand (QS) (expressed as wt.%) determined by X-ray fluorescence (XRF). (Standard deviation (SD) 0.02 wt.%).

| Oxide                          | AW    | ES    | MS    | DO    | QS    |
|--------------------------------|-------|-------|-------|-------|-------|
| Al <sub>2</sub> O <sub>3</sub> | 79.05 | –     | –     |       | 1.08  |
| SiO <sub>2</sub>               | 3.26  | 0.13  | 0.19  | 0.09  | 98.00 |
| MgO                            | 3.90  | 0.40  | 0.10  | 20.09 | 0.01  |
| TiO <sub>2</sub>               | 5.10  | –     | –     | –     | 0.57  |
| K <sub>2</sub> O               | 4.05  | 0.67  | 0.70  | 0.42  | 0.01  |
| CaO                            | 1.64  | 97.24 | 97.68 | 77.23 | 0.08  |
| Cl                             | 0.15  | 0.27  | 0.29  | 0.35  | –     |
| Na <sub>2</sub> O              | 1.00  | –     | 0.30  | 0.80  | 0.07  |
| ZrO <sub>2</sub>               | 0.74  | –     | –     | –     | –     |
| Fe <sub>2</sub> O <sub>3</sub> | 0.51  | 0.01  | 0.03  | 0.04  | 0.31  |
| SO <sub>3</sub>                | 0.24  | 0.98  | 0.45  | 0.09  | –     |
| ZnO                            | 0.09  | –     | –     | –     | –     |
| V <sub>2</sub> O <sub>5</sub>  | 0.12  | –     | –     | –     | –     |
| CuO                            | 0.05  | –     | –     | –     | –     |
| SrO                            | 0.03  | 0.05  | 0.20  | 0.03  | –     |
| MnO                            | 0.02  | –     | –     | 0.02  | 0.01  |

Figure 4 shows the XRD patterns of the raw materials. The aluminum waste is a complex and heterogeneous material composed principally of about 79 wt.% aluminum (expressed as Al<sub>2</sub>O<sub>3</sub>) which is distributed among different compounds such as metallic aluminum, aluminum nitride (AlN), corundum (Al<sub>2</sub>O<sub>3</sub>), and spinel (MgAl<sub>2</sub>O<sub>4</sub>) as the main Al-containing crystalline phases.

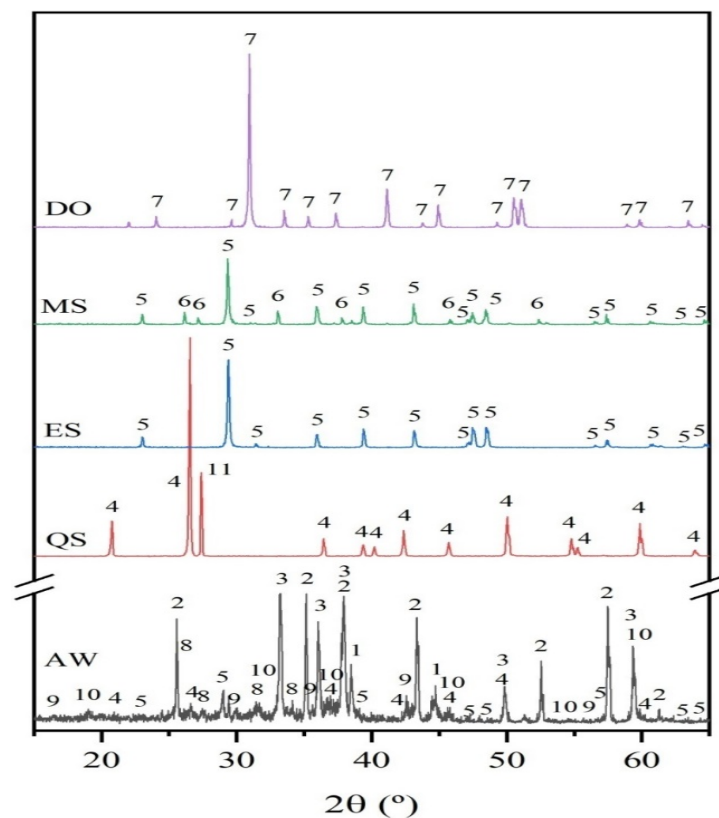


**Figure 4.** XRD patterns of raw materials: aluminum waste (AW), eggshells (ES), mussel shells (MS), dolomite (DO) and, quartz sand (QS) (1: Al, ICDD 00-004-0787; 2:  $\text{Al}_2\text{O}_3$  corundum, ICDD 00-046-1212; 3: AlN, ICDD 00-025-1133; 4:  $\text{SiO}_2$  quartz, ICDD 01-083-0539; 5:  $\text{CaCO}_3$  calcite, ICDD 00-005-0586; 6:  $\text{CaCO}_3$  aragonite, ICDD 00-041-1475; 7:  $\text{CaMg}(\text{CO}_3)_2$  dolomite, ICDD 01-089-5862; 8:  $\text{K}_4\text{H}_4\text{Si}_4\text{O}_{12}$ , ICDD 01-072-1101; 9:  $\text{Fe}_3\text{O}_4$  magnetite, ICDD 01-0075-1609; 10:  $\text{Al}_2\text{MgO}_4$  spinel, ICDD 01-073-2210; and, 11:  $\text{KAlSi}_3\text{O}_8$  microcline, ICDD 00-0010705).

The XRD profile of AW also shows the reflection corresponding to magnetite ( $\text{Fe}_3\text{O}_4$ ), calcite ( $\text{CaCO}_3$ ), and quartz ( $\text{SiO}_2$ ). Moreover, the presence of amorphous phases cannot be excluded because of the broad background of the XRD pattern. The chemical composition of eggshell and mussel shell is mainly comprised of calcium carbonate,  $\text{CaCO}_3$  (>97%, expressed as CaO); differences come, among others, from the morphology of the carbonate phases; thus, XRD profile of eggshell fits well to that of calcite and for mussels shell two polymorphs of calcium carbonate, calcite, and aragonite are observed. The XRD pattern of dolomite corresponds to that of  $\text{MgCa}(\text{CO}_3)_2$ . The XRD pattern of sand consists of quartz as the main crystalline phase, along with the minor phase microcline ( $\text{KAlSi}_3\text{O}_8$ ).

### 3.2. Thermal Behavior of Initial Mixtures

Prior to the treatment with concentrated solar energy, the thermal behavior of the three initial mixtures ( $M_i$ -ES,  $M_i$ -MS, and  $M_i$ -DO) was studied by DTA. The corresponding curves are depicted in Figure 5. The first exothermic peaks observed from room temperature to 560 °C for  $M_i$ -ES and  $M_i$ -MS, are attributed to different processes of combustion of the organic matter contained in eggshell and mussel shell. Besides, in the case of the  $M_i$ -MS sample, the endothermic peak at around 450 °C can be assigned to the phase transformation of aragonite to calcite [21–23]. After that, the decarbonation of calcium carbonate takes place as an endothermic process. The most intensive endothermic peak for all samples corresponds to that of decarbonation of calcite, which occurs in the case of ES and MS at higher temperature (894 and 890 °C, respectively) than that corresponding to sample with DO (851 °C). The decarbonation of dolomite occurs in two steps: the first, at 651 °C,

is due to the partial decarbonation of  $\text{CaMg}(\text{CO}_3)_2$  to form periclase ( $\text{MgO}$ ) and calcite ( $\text{CaCO}_3$ ); and, the second, at  $851^\circ\text{C}$ , corresponds to the decarbonation of calcite to form lime ( $\text{CaO}$ ) [24,25]. Up to the maximum recorded temperature ( $1200^\circ\text{C}$ ), the endothermic fall indicative of the formation of liquid phases is not observed in any case. The formation of liquid phases is necessary to promote the melting of the raw materials, and accordingly temperatures much higher than  $1200^\circ\text{C}$  must have been reached in the melting process with CSE, as above indicated.

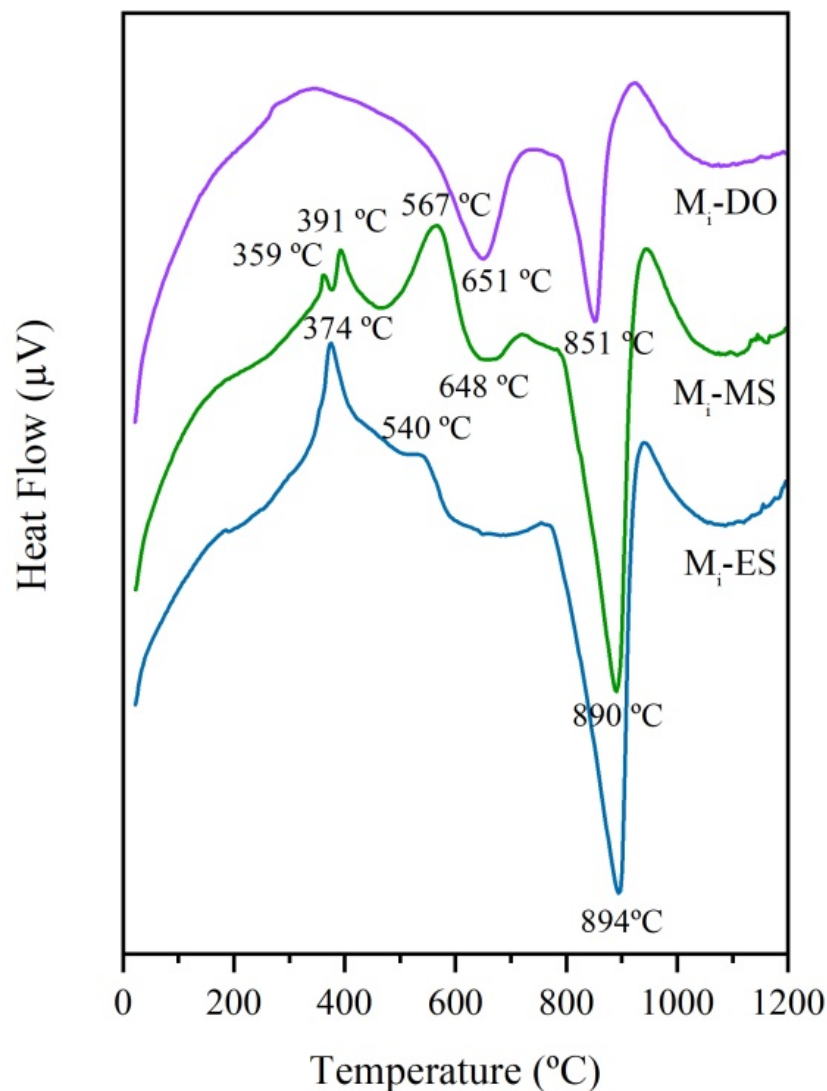


**Figure 5.** DTA curves of initial mixtures:  $M_i$ -ES,  $M_i$ -MS, and  $M_i$ -DO.

### 3.3. Characterization of Samples Obtained by CSE

The macroscopic aspect of the samples (glass frits) obtained after different times of exposure to solar radiation are depicted in Figure 6. The samples obtained with an exposure time of 5 min exhibit a clear opacity and lack of clarity, which could indicate that the reactions between the different components of raw materials were not completed. However, in  $M_5$ -ES, several well-vitrified areas are distinguished. For longer exposure times, the macroscopic appearance of frits looks like glasses. According to these observations, 5 min is a very short time to allow complete decarbonation and melting reactions. Periods of time of 10 min or longer are required. All glass frits were green in color and transparent and, appreciable differences were not observed between the frits prepared from the different initial mixtures. Durham and Risbud [26] described green-colored glasses for silica-calcium-aluminate-oxinitride glasses obtained from chemical reagents at  $1700^\circ\text{C}$ . Shelby [27] also

reported colored glasses in the calcium-aluminate system, especially for high CaO content. This author considers that the color results from an increase in absorption over the entire visible region rather than being associated with any specific absorption band. In our case, the glasses color could be also attributed to the presence of metallic oxides (iron, copper, etc.) [16]. However, it is noticeable that the samples prepared with the shortest exposure time show a darker color than those prepared with longer exposure times. This difference is probably due, as explained below, to the different glassy character of the samples. Thus, the samples prepared at 5 min contain crystals dispersed in an amorphous phase. The higher refractive indices of the crystalline phases with respect to the glass cause a decrease in the reflected light and, therefore, the samples prepared at 5 min show less luminosity and their color is perceived as darker.

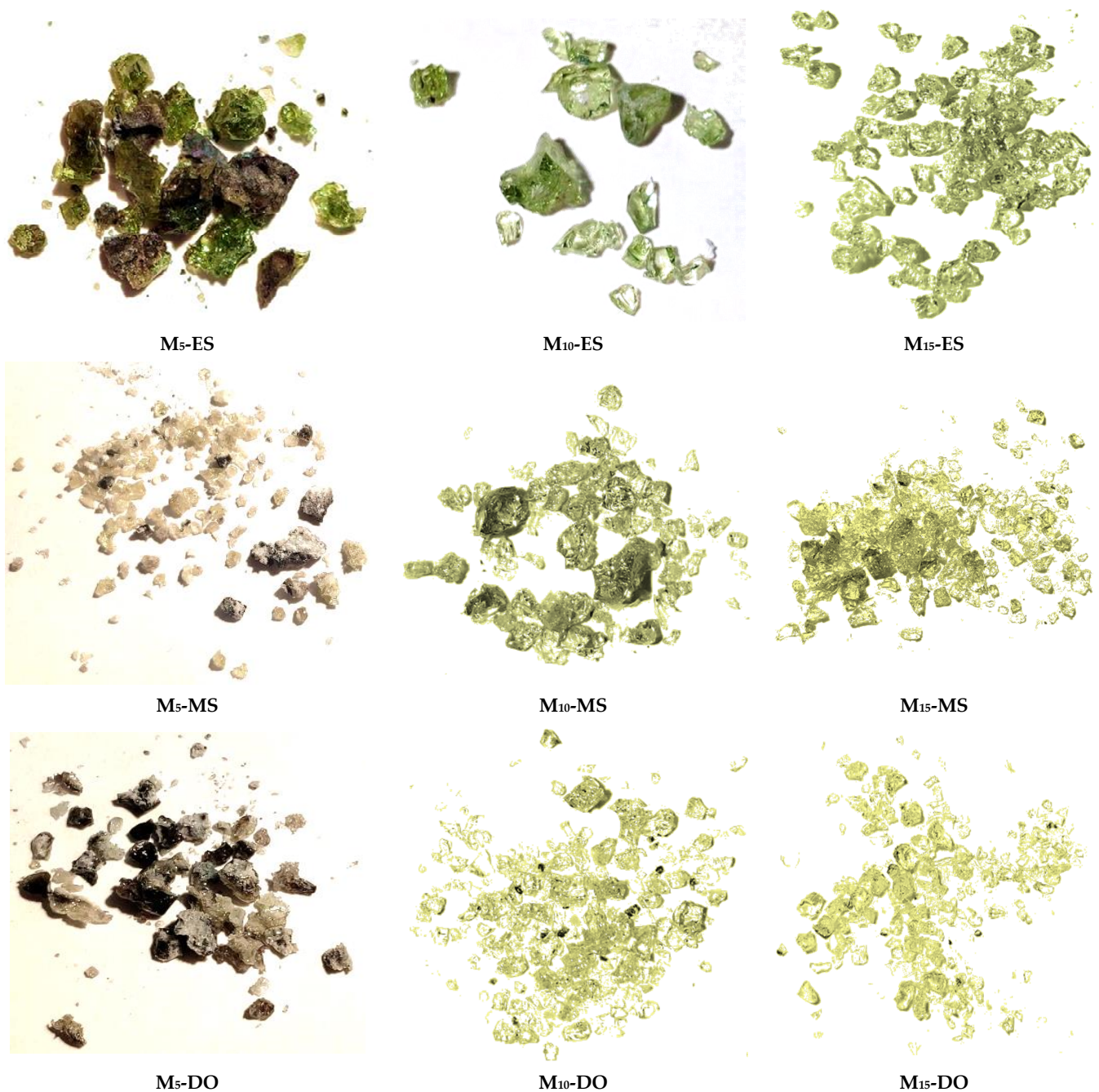


Figure 6. Macroscopic appearance of the frits obtained by CSE.



### 3.3.1. Chemical Composition

The chemical composition of glasses prepared by melting the initial mixtures for 15 min of exposure to solar radiation is collected in Table 3. The samples obtained at low periods of exposure were not considered for this analysis because they showed less amorphous character as will be discussed later. Based on these compositions, although the initial mixtures were formulated in the SiO<sub>2</sub>-Al<sub>2</sub>O<sub>3</sub>-CaO system, different elements, such as magnesium, titanium, iron, alkalines, etc., mainly from aluminum waste are also incorporated in the glass network as modifiers.

**Table 3.** Main composition of the glasses obtained after 15 min of exposure to concentrated solar energy (CSE) (XRF, expressed as oxides in wt.%; SD 0.02 wt.%).

| Compounds                      | M <sub>15</sub> -ES | M <sub>15</sub> -MS | M <sub>15</sub> -DO |
|--------------------------------|---------------------|---------------------|---------------------|
| SiO <sub>2</sub>               | 34.09               | 41.85               | 39.22               |
| Al <sub>2</sub> O <sub>3</sub> | 23.03               | 22.49               | 24.34               |
| CaO                            | 36.27               | 30.41               | 21.91               |
| MgO                            | 1.30                | 1.00                | 9.20                |
| TiO <sub>2</sub>               | 1.83                | 1.50                | 1.82                |
| K <sub>2</sub> O               | 0.95                | 0.73                | 0.89                |
| Na <sub>2</sub> O              | 0.70                | 0.40                | 0.70                |
| Cl                             | 0.50                | 0.47                | 0.61                |
| SO <sub>3</sub>                | 0.47                | 0.38                | 0.48                |
| Fe <sub>2</sub> O <sub>3</sub> | 0.37                | 0.37                | 0.41                |
| ZrO <sub>2</sub>               | 0.29                | 0.24                | 0.27                |
| CuO                            | 0.03                | 0.02                | 0.02                |
| SrO                            | 0.04                | 0.08                | 0.02                |
| ZnO                            | 0.01                | <<0.01              | 0.02                |
| SnO <sub>2</sub>               | 0.01                | 0.01                | 0.01                |
| Cr <sub>2</sub> O <sub>3</sub> | 0.02                | <0.01               | <0.01               |
| MnO                            | 0.02                | <<0.01              | <<0.01              |

The Al<sub>2</sub>O<sub>3</sub> content is similar in the three glasses and the main differences in composition are in the silica and alkaline-earth oxides contents. The SiO<sub>2</sub> content in the M<sub>15</sub>-DO and M<sub>15</sub>-MS glasses is higher than in the M<sub>15</sub>-ES glass, which is likely due to the formation of more corrosive melts and their subsequent incorporation from the crucible walls. Concerning alkaline-earth oxides, the differences observed in the M<sub>15</sub>-DO when compared to the M<sub>15</sub>-MS and M<sub>15</sub>-ES are due to the high magnesium content in dolomite.

Figure 7 depicts the location of the composition of the M<sub>15</sub>-DO, M<sub>15</sub>-MS, and M<sub>15</sub>-ES glasses in the SiO<sub>2</sub>-Al<sub>2</sub>O<sub>3</sub>-CaO ternary phase diagram. The composition of M<sub>15</sub>-DO is placed within the area of anorthite (CaAl<sub>2</sub>Si<sub>2</sub>O<sub>8</sub>) formation. This region also contains the glass prepared with mussel shell, although it is located in a zone of temperature lower than that of the glass prepared with dolomite (1400 °C for M<sub>15</sub>-MS and around 1500 °C for M<sub>15</sub>-DO). Regarding the chemical composition of glass M<sub>15</sub>-ES, it is fitted in the region of gehlenite (Ca<sub>2</sub>Al<sub>2</sub>SiO<sub>7</sub>) formation, as a consequence of its higher calcium content.

### 3.3.2. Powder X-Ray Diffraction Analysis

The XRD patterns and the crystalline degree of frits obtained by CSE after different exposure time to solar radiation are depicted in Figures 8 and 9, respectively. In general, the characteristic halo of amorphous materials is detected for all samples, but several diffraction peaks due to crystalline phases are observed, especially in the samples prepared at the shortest treatment time (5 min). Depending on the source of calcium employed (eggshell, mussel shell or dolomite) different crystalline phases are discerned in the corresponding XRD patterns, and different evolution of the amorphous halo with the treatment time is also observed. In general, the shorter time of 5 min leads to non-glassy materials, as denoted by the presence of different crystalline phases, both from remaining raw material

phases and from neo-formation phases (Figure 8). This fits well with the high crystallinity determined by EVA program, with values ranging from 30 to 50% (Figure 9).

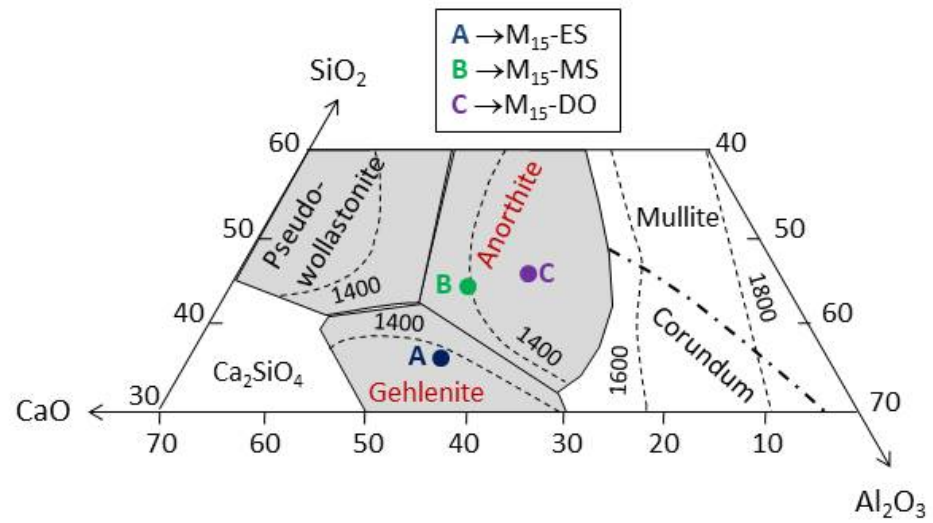


Figure 7.  $\text{SiO}_2$ - $\text{Al}_2\text{O}_3$ -CaO ternary phase diagram. [28].

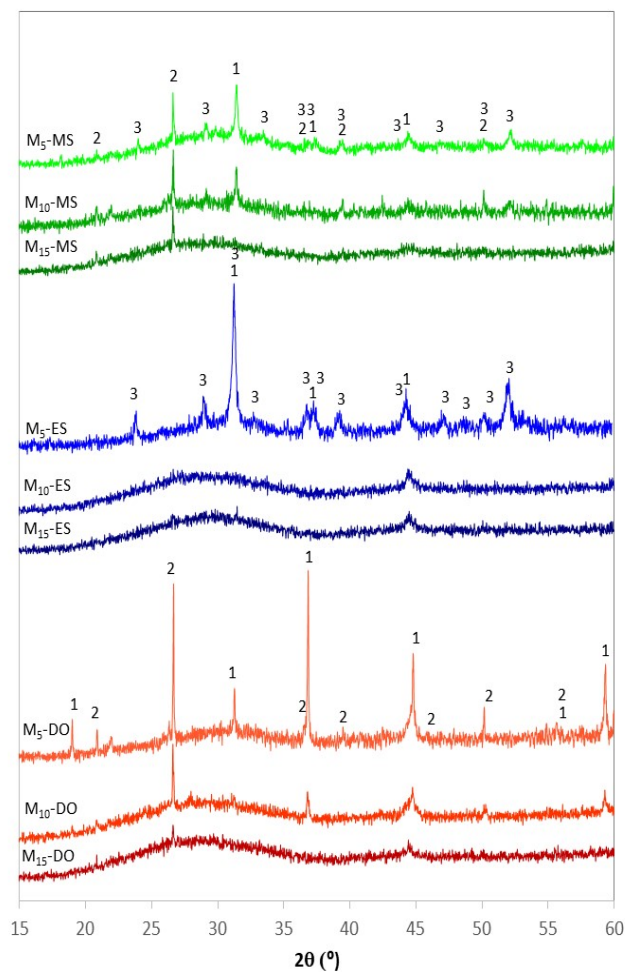
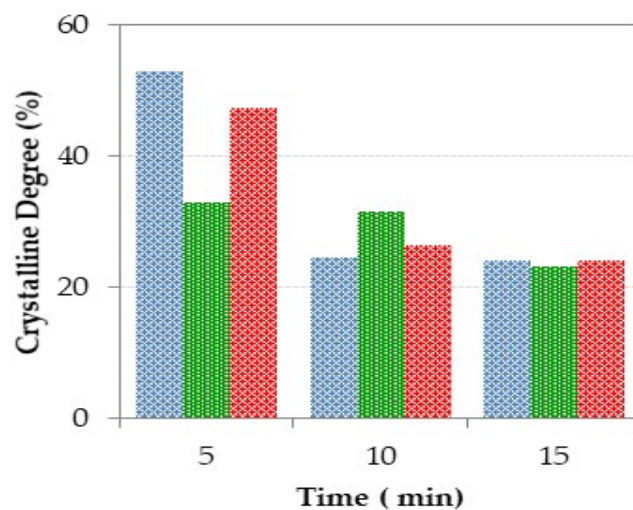


Figure 8. XRD patterns of the samples obtained by CSE at different treatment time. (1:  $\text{MgAl}_2\text{O}_4$  spinel, ICDD 01-086-0085; 2:  $\text{SiO}_2$  quartz, ICDD 01-083-0539; 3:  $\text{Ca}_2\text{Al}_2\text{SiO}_7$  gehlenite, ICDD 01-079-1726).



**Figure 9.** Percentage of crystallinity of the glasses prepared using CSE for different radiation exposure time (blue: M<sub>x</sub>-ES, green: M<sub>x</sub>-MS and, red: M<sub>x</sub>-DO).

For the materials prepared with dolomite, the XRD profile at 5 min denotes the existence of quartz coming from the sand, which indicates that this time, is not enough to achieve its complete incorporation into the melt during the treatment with solar energy. Moreover, well-defined peaks attributed to spinel are detected in the XRD pattern. This phase could be a remain of the spinel contained in the AW, but the intensity of the peaks compared to those in the AW pattern indicates that probably the spinel is a new formation phase, which could be promoted by the higher magnesium content in the sample obtained from dolomite. As the exposure time increases, the amorphous character of the samples also increases. Thus, the presence of only two very weak peaks due to quartz and spinel, which are the most refractory phases, was observed for the sample obtained after 15 min. Regarding the crystalline degree, Figure 9 denotes a very significant decrease for samples obtained at 10 and 15 min (26.6 and 24.2%, respectively) in relation to the samples obtained at shorter time.

In the case of the samples prepared from eggshell, the XRD profile at 5 min also shows the presence of crystalline phases, but now, the main phase is gehlenite (Ca<sub>2</sub>Al<sub>2</sub>SiO<sub>7</sub>, ICDD 01-079-1726), which is a neo-formation phase developed by solid state reaction from the aluminum compounds (from aluminum waste), quartz (from quartz sand), and calcite (from eggshell). The formation of gehlenite agrees with the SiO<sub>2</sub>-Al<sub>2</sub>O<sub>3</sub>-CaO ternary diagram (Figure 7), since the chemical composition of M<sub>x</sub>-ES materials is placed within the region of gehlenite formation. However, the development of gehlenite has not been observed in samples prepared with dolomite, likely due to the lower calcium content in the initial mixtures. The development of gehlenite leads to the high crystallinity of this sample (52.9%). M<sub>10</sub>-ES and M<sub>15</sub>-ES exhibit similar amorphous DRX profile with a weak peak at 44.45° (2θ), which may be tentatively attributed to the 400 hkl reflection of a non-stoichiometric spinel (Mg<sub>0.4</sub>Al<sub>2.4</sub>O<sub>4</sub>, reference file ICDD 01-086-0085). The crystalline grade of these samples is also similar (~24.5%).

Regarding the samples prepared from mussel shell, the XRD pattern at 5 min shows the presence of quartz and spinel in a similar way to M<sub>5</sub>-DO sample, although in this case the crystalline degree is lower (33%) as denoted by the low intensity of the corresponding diffraction reflections and the high intensity of the amorphous halo. Besides, weak peaks attributed to gehlenite are also observed. According to the SiO<sub>2</sub>-Al<sub>2</sub>O<sub>3</sub>-CaO ternary diagram (Figure 7) the gehlenite formation was not expected, since the chemical composition of M<sub>5</sub>-MS is located in the region of anorthite formation. Nevertheless, it should be noted that the compositions represented in the diagram are not the true quantitative composition of the samples because only the CaO, Al<sub>2</sub>O<sub>3</sub>, and SiO<sub>2</sub> contents were taken into account. M<sub>5</sub>-MS sample also contain minor elements (Na, K, Ti, . . . ) which could shift its location

toward the region of gehlenite formation. As the time increases, the amorphous character of the resulting samples increases, and consequently, the crystalline degree decreases (31.6 and 23.2% for samples obtained with 10 and 15 min treatments, respectively).

According to XRD results, the use of eggshell as calcium source (calcite) might require shorter exposure time than those required for mussel shell (calcite and aragonite) or dolomite (double calcium/magnesium carbonate).

### 3.3.3. Differential Thermal Analysis of Glasses

Figure 10 depicts the DTA curves of glass frits prepared by CSE for 15 min of solar radiation exposure. The first endothermic fall corresponds to the glass thermal transition ( $T_g$ ), which varies in the 732–775 °C range. The  $T_g$  value is affected by both the glass chemical composition and its thermal history. In this study, the three glasses were prepared following the same heating and cooling process. Thus, the small variations observed in the  $T_g$  values must be due to the differences in the chemical composition. In fact, as seen in Table 3, the glasses mainly differ in their  $\text{SiO}_2$ ,  $\text{MgO}$ , and  $\text{CaO}$  content. After that, the three DTA curves depict an exothermic growth, which is indicative of a devitrification process and the subsequent development of crystalline phases. In this context, some differences in the behavior of the three glasses are observed.

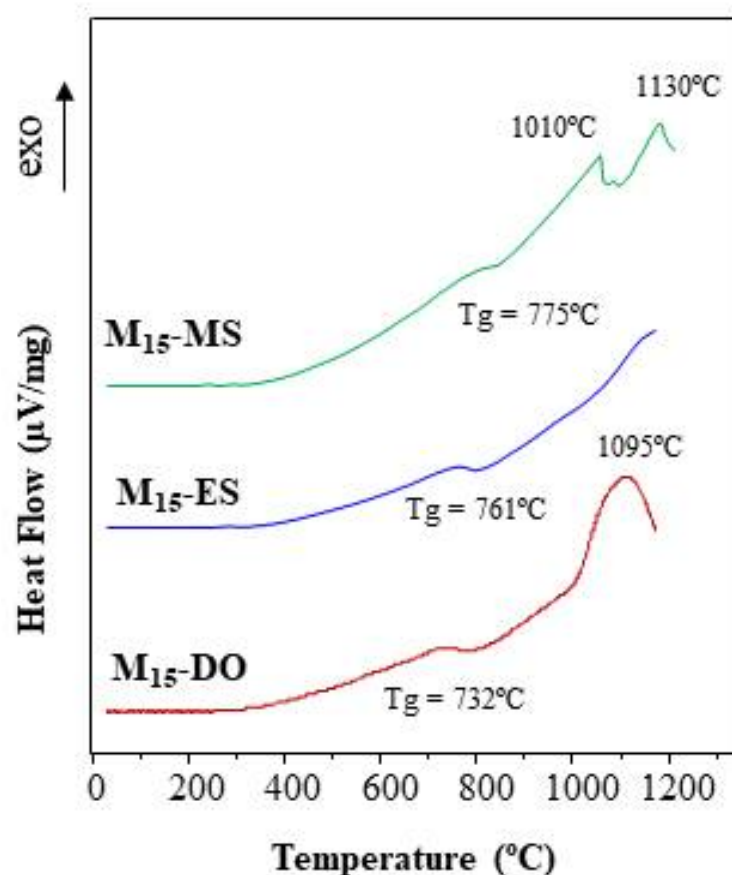


**Figure 10.** DTA curves of glasses prepared by CSE.

The DTA curve of the  $M_{15}$ -DO glass exhibits an exothermic peak centered at 1095 °C, which could be assigned to the formation of anorthite according to the ternary diagram (Figure 7). Similarly, the  $M_{15}$ -ES glass depicts an exothermic rise, but the maximum is not clearly reached in the studied temperature range (up to 1165 °C). This exothermic effect could be attributed to gehlenite development. Concerning  $M_{15}$ -MS glass, two crystallization peaks are distinguished in the exothermic process (1010 and 1130 °C). The chemical composition of this glass is located in the region of anorthite formation. However, the



mineralogical study (Figure 8) has highlighted the possibility of gehlenite crystallization. In this way, the two exothermic peaks could be attributed to the development of anorthite (peak at 1010 °C) and gehlenite (peak at 1130 °C). The results indicate that the glasses are thermally unstable and are able to develop crystalline phases after a thermal treatment. Thus, the use of eggshell, mussel shell, or dolomite as calcium source might be selected according to the crystalline phase expected to be developed during the devitrification of the glasses.

#### 4. Conclusions

The results of this study indicate the ability of the use of concentrated solar energy to manufacture glasses formulated from different waste materials as raw materials. These include a hazardous aluminum waste as alumina source and food industry waste as CaO source, among other components. The glasses obtained are located in the areas of gehlenite and anorthite formation in the ternary SiO<sub>2</sub>-Al<sub>2</sub>O<sub>3</sub>-CaO system, with values of glass thermal transition temperature ranging in the 732–775 °C interval.

The use of concentrated solar energy could be considered as a promising option to reduce the cost of the vitrification process of waste. Calcination and melting of raw materials are performed at short exposure time and, consequently, important cost savings may be achieved. Besides, waste vitrification could be understood as a process to obtain added value materials, rather than as a mere process to render inert materials. Nevertheless, many experiments must be still carried out in this research line to optimize the melting process and the solar radiation concentration system, in order to be able to up-scale the process for the melting of large volume of waste.

**Author Contributions:** The authors contributions are as follow: Conceptualization, M.R. and A.L.-D.; methodology, A.L.-D. and J.I.R.; investigation, I.P., M.R. and A.L.-D.; writing—original draft preparation, A.L.-D. and M.R.; writing—review and editing, A.L.-D., M.R. and I.P.; supervision, M.R., I.P. and A.L.-D.; project administration, M.R. and A.L.-D.; funding acquisition, M.R. and A.L.-D. All authors have read and agreed to the published version of the manuscript.

**Funding:** This research was funded by Spanish Science and Innovation Ministry, grant number ECLICESOL-Mat2017-83025-R and, by European Solar Research Infrastructure for Concentrated Solar Power SFERA-III program" (EU.DG RTD's), grant number FIGARO-SURPF1904010021.

**Institutional Review Board Statement:** Not applicable.

**Informed Consent Statement:** Not applicable.

**Data Availability Statement:** Not applicable.

**Conflicts of Interest:** The authors declare no conflict of interest. The funders had no role in the design of the study; in the collection, analyses, or interpretation of data; in the writing of the manuscript, or in the decision to publish the results.

#### References

1. Plaza, D.M.; Martinez, I.C.; Gasch, G.M.; Sufrategui, F.T.; García, J.R. A case study of the feasibility of using solar concentrating technologies for manufacturing ceramics. *J. Clean. Prod.* **2015**, *87*, 977–991. [CrossRef]
2. Scalet, B.M.; Garcia Muñoz, M.; Sissa Aivi, Q.; Roudier, S.; Luis, D.S. *Best Available Techniques (BAT) Reference Document for the Manufacture of Glass*; Publications Office of the European Union: Luxembourg, 2013; ISBN 9789279282843.
3. Trends in Atmospheric Carbon Dioxide. Available online: [https://www.esrl.noaa.gov/gmd/ccgg/trends/gl\\_trend.html](https://www.esrl.noaa.gov/gmd/ccgg/trends/gl_trend.html) (accessed on 23 February 2021).
4. United Nations Sustainable Development Goals. Available online: <https://www.un.org/sustainabledevelopment/sustainable-development-goals/> (accessed on 24 February 2021).
5. McMillan, P.; Piriou, B.; Navrotsky, A. A Raman spectroscopic study of glasses along the joins silica-calcium aluminate, silica-sodium aluminate, and silica-potassium aluminate. *Geochimica Cosmochimica Acta* **1982**, *46*, 2021–2037. [CrossRef]
6. Navrotsky, A.; Peraudeau, G.; McMillan, P.; Coutures, J.P. A thermochemical study of glasses and crystals along the joins silica-calcium aluminate and silica-sodium aluminate. *Geochimica Cosmochimica Acta* **1982**, *46*, 2039–2047. [CrossRef]
7. McMillan, P.; Piriou, B. The structures and vibrational spectra of crystals and glasses in the silica-alumina system. *J. Non. Cryst. Solids* **1982**, *53*, 279–298. [CrossRef]

8. Romero, M.; Robla, J.I.; Padilla, I.; García-Hierro, J.; López-Delgado, A. Eco-efficient melting of glass frits by concentrated solar energy. *Sol. Energy* **2018**, *174*, 321–327. [[CrossRef](#)]
9. López-Delgado, A.; Tayibi, H.; Pérez, C.; Alguacil, F.J.; López, F.A. A hazardous waste from secondary aluminium metallurgy as a new raw material for calcium aluminate glasses. *J. Hazard. Mater.* **2009**, *165*, 180–186. [[CrossRef](#)] [[PubMed](#)]
10. Scarinci, G.; Brusatin, G.; Barbieri, L.; Corradi, A.; Lancellotti, I.; Colombo, P.; Hreglich, S.; Dall'Igna, R. Vitrification of industrial and natural wastes with production of glass fibres. *J. Eur. Ceram. Soc.* **2000**, *20*, 2485–2490. [[CrossRef](#)]
11. Guzmán-Carrillo, H.R.; Pérez, J.M.; Aguilar Reyes, E.A.; Romero, M. Coal fly ash and steel slag valorisation throughout a vitrification process. *Int. J. Environ. Sci. Technol.* **2018**, *15*, 1757–1766. [[CrossRef](#)]
12. Bernardo, E.; Varrasso, M.; Cadamuro, F.; Hreglich, S. Vitrification of wastes and preparation of chemically stable sintered glass-ceramic products. *J. Non. Cryst. Solids* **2006**, *352*, 4017–4023. [[CrossRef](#)]
13. Higby, P.L.; Ginther, R.J.; Aggarwal, I.D.; Friebele, E.J. Glass formation and thermal properties of low-silica calcium aluminosilicate glasses. *J. Non. Cryst. Solids* **1990**, *126*, 209–215. [[CrossRef](#)]
14. Cormier, L.; Neuville, D.R.; Calas, G. Structure and properties of low-silica calcium aluminosilicate glasses. *J. Non. Cryst. Solids* **2000**, *274*, 110–114. [[CrossRef](#)]
15. Weber, J.K.R.; Tangeman, J.A.; Key, T.S.; Hiera, K.J.; Paradis, P.F.; Ishikawa, T.; Yu, J.; Yoda, S. Novel synthesis of calcium oxide-aluminum oxide glasses. *Jpn. J. Appl. Phys.* **2002**, *41*, 3029–3030. [[CrossRef](#)]
16. Galindo, R.; Padilla, I.; Sánchez-Hernández, R.; Robla, J.I.; Monrós, G.; López-Delgado, A. Production of added-value materials from a hazardous waste in the aluminium tertiary industry: Synergistic effect between hydrotalcites and glasses. *J. Environ. Chem. Eng.* **2015**, *3*, 2552–2559. [[CrossRef](#)]
17. Teixeira, S.R.; Magalhães, R.S.; Arenales, A.; Souza, A.E.; Romero, M.; Rincón, J.M. Valorization of sugarcane bagasse ash: Producing glass-ceramic materials. *J. Environ. Manage.* **2014**, *134*, 15–19. [[CrossRef](#)]
18. Galindo, R.; Padilla, I.; Rodríguez, O.; Sánchez-Hernández, R.; López-Andrés, S.; López-Delgado, A. Characterization of Solid Wastes from Aluminum Tertiary Sector: The Current State of Spanish Industry. *J. Miner. Mater. Charact. Eng.* **2015**, *3*, 55–64. [[CrossRef](#)]
19. Romero, M.; Martín, M.I.; Barbieri, L.; Andreola, F.; Lancellotti, I.; López-Delgado, A. Valorization of Al slag in the production of green ceramic tiles: Effect of experimental conditions on microstructure and crystalline phase composition. *J. Am. Ceram. Soc.* **2020**, *104*, 776–784. [[CrossRef](#)]
20. Procédés, Matériaux et Énergie Solaire. Available online: <https://www.promes.cnrs.fr/index.php?page=home-en> (accessed on 30 September 2020).
21. Yoshioka, S.; Kitano, Y. Transformation of aragonite to calcite through heating. *Geochem. J.* **1985**, *19*, 245–249. [[CrossRef](#)]
22. Hamester, M.R.R.; Balzer, P.S.; Becker, D. Characterization of calcium carbonate obtained from oyster and mussel shells and incorporation in polypropylene. *Mater. Res.* **2012**, *15*, 204–208. [[CrossRef](#)]
23. Zhang, Y.; Wu, H.L.S. Analysis on the properties of calcined waste mussel shell. *Anal. Chem. Indian J.* **2013**, *13*, 167–171.
24. Rat'Ko, A.I.; Ivanets, A.I.; Kulak, A.I.; Morozov, E.A.; Sakhar, I.O. Thermal decomposition of natural dolomite. *Inorg. Mater.* **2011**, *47*, 1372–1377. [[CrossRef](#)]
25. Valverde, J.M.; Perejon, A.; Medina, S.; Perez-Maqueda, L.A. Thermal decomposition of dolomite under CO<sub>2</sub>: Insights from TGA and in situ XRD analysis. *Phys. Chem. Chem. Phys.* **2015**, *17*, 30162–30176. [[CrossRef](#)] [[PubMed](#)]
26. Durham, J.; Risbud, G. Low silica calcium aluminate oxynitride glasses. *Mater. Lett.* **1988**, *7*, 208–210. [[CrossRef](#)]
27. Shelby, J.E. Formation and properties of aluminosilicate glasses. *J. Am. Ceram. Soc.* **1985**, *68*, 155–158. [[CrossRef](#)]
28. Höland, W.; Beal, G.H. *Glass-Ceramic Technology*, 2nd ed.; The American Ceramic Society: Hoboken, NJ, USA, 2012; ISBN 9781118265987.